Pergamon

Geochimica et Cosmochimica Acta, Vol. 67, No. 23, pp. 4471–4487, 2003

0016-7037/03 $30.00 + .00

doi:10.1016/S0016-7037(03)00413-7

Lead sorption efficiencies of natural and synthetic Mn and Fe-oxides

S. E. O'Reilly*,† and Michael F. Hochella, Jr.

NanoGeoscience and Technology Laboratory, Department of Geological Sciences, 4044 Derring Hall, Virginia Tech, Blacksburg, VA 24061, USA

(*Received November* 6, 2002; *accepted in revised form June* 5, 2003)

Abstract—Lead sorption efficiencies (sorption per specific surface area) were measured for a number of natural and synthetic Mn and Fe-oxides using a flow-through reactor. The Mn-oxide phases examined included synthetic birnessite, natural and synthetic cryptomelane, and natural and synthetic pyrolusite; the Fe-oxides studied were synthetic akaganéite, synthetic ferrihydrite, natural and synthetic goethite, and natural and synthetic hematite. The sorption flow study experiments were conducted with 10 ppm Pb with an ionic strength of either 0.01 M $NaNO_3$ or 0.01 M KNO_3, both at pH 5.5. The experimental effluent solution was analyzed using aqueous spectroscopic methods and the reacted solids were analyzed using microscopy (field emission scanning electron microscopy, FE-SEM), structure analysis (powder X-ray diffraction, XRD), bulk chemical spectroscopy (energy dispersive spectroscopy, EDS), and surface sensitive spectroscopy (X-ray photoelectron spectroscopy, XPS). Overall and under these conditions, the synthetic Mn-oxides have higher sorption efficiencies than the natural Mn-oxides, which in turn are higher than the natural and synthetic Fe-oxides. Only natural pyrolusite had a sorption efficiency as low as the Fe-oxides. Most of the natural and synthetic Fe-oxides examined in this study removed about the same amount of Pb from solution once normalized to BET N_2 surface area, although synthetic akaganéite and hematite were significantly less reactive than the rest.

It is suggested that the observed efficiency of Mn-oxides for Pb sorption is directly related to internal reactive sites in the structures that contain them (birnessite and cryptomelane, in the case of this study). Comparisons of solution data to XPS data indicated that Pb went into the interlayer of the birnessite, which was supported by XRD; similarly some Pb may go into the tunnels of the cryptomelane structure. Layer structures such as birnessite have the highest Pb sorption efficiency, while the 2×2 tunnel structure of cryptomelane has lower efficiencies than birnessite, but higher efficiencies than other Mn- or Fe-oxide structures without internal reactive sites.

1. INTRODUCTION

Manganese oxides are typically thought to be the most important scavengers of aqueous trace metals in soils, sediments, and rocks through their seemingly dominant sorptive behavior despite the fact that they are much less abundant than iron oxides (e.g., Jenne, 1968; Burns, 1976; Chao and Theobald, 1976; Schwertmann and Taylor, 1989). In both the cases of Mn and Fe-oxides, their reactivity and generally high surface areas make them proficient sorbents of many inorganic cations such as Cu, Pb, Zn, Co, and Ni, among others (e.g., Jenne, 1968; McKenzie, 1980; Schwertmann and Taylor, 1989; McBride, 1994). In particular, manganese (III/IV) and iron (III) oxide/hydroxide mineral particles and coatings in soils seem to have a strong affinity for Pb (Rickard and Nriagu, 1978), and soils represent the major near surface sink for anthropogenic sources of this metal (Nriagu, 1978). Thus these minerals may be able to effectively sequester Pb, one of the most common (Nriagu, 1978) and extensively distributed toxic metals in the environment (Boeckx, 1986; Kaim, 1994).

Research has shown that Pb collects in soil Mn-oxides (Norrish, 1975), and when Mn-oxide was added to Pb contaminated soils, Pb uptake by plants was reduced (McKenzie, 1978). Several studies have also shown that Pb sorption was greater than for other metals, including Ba, Cd, Co, Cu, Mn, Ni, and Zn on various Mn-oxides (Gadde and Laitinen, 1974; Van der Weijden and Kruissink, 1977; McKenzie, 1980; Aualiitia and Pickering, 1987; Parida et al., 1996). Additionally, other studies have indicated that Mn-oxides generally sorbed more Pb than other phases such as Fe-oxides, Al-oxides, organics or clays (Gadde and Laitinen, 1974; McKenzie, 1980; Aualiitia and Pickering, 1987; Dong et al., 2000). Hudson-Edwards (2000) also found that Mn-oxides in sediments did contain considerably more Pb than Fe-oxides. Finally and not surprisingly, it is common for authors, in reviewing the literature, to state that Pb is preferentially accumulated by Mn-oxides (e.g., Nriagu, 1978; Balistrieri and Murray, 1986; Paulson et al., 1988; Manceau et al., 1992; Dahal and Lawrance, 1996; Morin et al., 1999).

Unfortunately, some of this information reviewed above seems to have been misleadingly propagated though the literature. When discussing Pb uptake, many papers cite the excellent review by Jenne (1968). However, this study did not investigate the role of hydrous Mn and Fe oxides on Pb concentrations in soils and waters, but instead Mn, Fe, Co, Ni, Cu, and Zn. Further, Taylor and McKenzie (1966) concluded from soil extraction studies that, even though Co, Ni, Mo, Ba, Zn, V, Cr, and Pb tend to be more concentrated in manganese minerals than whole soils, only Co seemed to have a major specific affinity for the Mn-oxide fraction of the soil. The authors did not find a linear correlation between the Pb content and the soil Mn fractions. Kabata-Pendias (1980) found that Pb was "fixed"

* Author to whom correspondence should be addressed (eoreilly@nrlssc.navy.mil).
† *Present address:* Naval Research Laboratory, Code 7431, Building 1005, Stennis Space Center, MS 39529 USA.

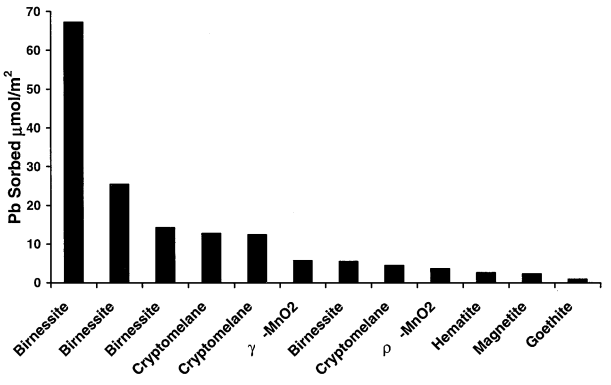

Fig. 1. Lead sorption to Mn and Fe-oxides in terms of surface area of the solid. Adapted from McKenzie (1980). The same phase is listed more than once because these solids were prepared using different synthesis methods.

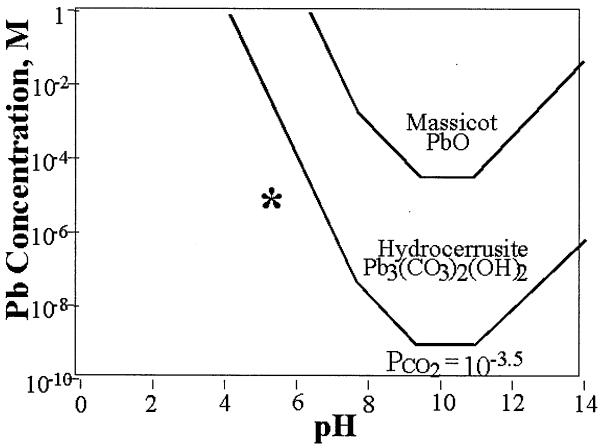

Fig. 2. Lead solubility diagram showing pH and Pb concentration at which the lead solids massicot and hydrocerrusite form at atmospheric carbonate levels. The asterisk approximately indicates the pH and Pb concentration conditions of this study. The thermodynamic data was obtained from Garrels and Christ (1965).

by Mn-oxides along with Zn and Cd, but Pb was also easily "fixed" by Fe-oxides. A study by Ostergren et al. (1999) discovered that in natural, contaminated samples Fe-oxides play a much more substantial role in the adsorption of Pb than Mn-oxides do.

Other studies also failed to find a correlation between Pb and Mn-oxides. Li (1982) conducted enrichment calculations on elements of manganese nodules and related sediments and concluded that Pb is concentrated in the Fe-oxides, not the Mn-oxides in the nodules. A study by Carpenter et al. (1975) evaluated the concentration of certain metals in the black coatings on stream boulders and showed that the coatings effectively reflected Zn and Cu mineralization in drainage basins, but not Pb. Lead was not concentrated in the coatings. Most recently, Dong et al. (2001) noted that there are different views on the importance of Mn-oxides, Fe-oxides, and even organic matter in trace metal uptake.

Clearly there are discrepancies in the literature as to whether Mn-oxides are particularly efficient at sorbing Pb, and beyond that, if they are more efficient at sequestering Pb than Fe-oxides. We have only found one paper by McKenzie (1980) that examined the sorption of Pb on multiple synthetic Mn-oxides in comparison to synthetic Fe-oxides and, for a portion of the study, looked at the Pb uptake of these solids normalized to their surface area (BET or otherwise). All of this work was done in batch reactors. In Figure 1, which was adapted from McKenzie (1980), we show the sorption of the various solids normalized to specific surface area. McKenzie's data show that the synthetic Mn-oxides sorb considerably more Pb per specific surface area than the Fe-oxides, and in one case dramatically so with the difference approaching two orders of magnitude. It is also apparent that the amount of Pb sorbed was greatly affected by the synthesis method of the solid. No evidence was found for the oxidation of Pb(II) to Pb(IV) nor for the formation of new solid phases. X-ray diffraction studies provided some evidence that Pb went into the interlayer of birnessite, which explained the high sorption capacity exhibited by some of the birnessite samples.

The types of studies that exist correlating Pb to Mn-oxides in soils fall into three categories: (1) extraction or selective extraction studies, (2) microprobe studies, and (3) sorption studies. All of these studies have increased our knowledge of these systems. However, extraction studies are plagued with artifacts such as removal of one or more phases in addition to the target phase, and also the potential redistribution of Pb species among other minerals in the sample (Taylor and McKenzie, 1966; Chao and Theobald, 1976; McCarty et al., 1998; Ostergren et al., 1999; Gilmore et al., 2001). Microprobe techniques are not surface sensitive and can be restricted by their detection limits for trace elements such as Pb (see Goldstein et al., 1992; Ostergren et al., 1999; Rauch et al., 2000). Sorption studies are often much more controlled than the extraction or microprobe studies because pure Mn-oxides are specifically synthesized for these studies. However, these synthetic phases have not been compared to natural phases to see how good of a proxy they are for the environment. The sorption studies often only examine a few minerals at best. They rarely compare multiple synthetic Mn-oxide phases to the "same" minerals collected in nature or directly to Fe-oxides. Even fewer of these studies normalize their data to the surface area of the solids tested, and this may be the cause of some of the contradictions in the literature.

Thus, the goals of our study are to (1) thoroughly examine the Pb sorption efficiency (i.e., amount sorbed per specific surface area) of several synthetic and natural Mn and Fe-oxides using well-characterized samples and flow-through reactor techniques, (2) obtain insight into what factors determine Pb sorption efficiency, and (3) clarify as many ambiguities or misconceptions in the existing literature as possible.

Lead sorption studies were conducted using a flow-through reactor so that chemical steady state conditions could be maintained during the experiments (Rimstidt and Newcomb, 1993; Sparks, 1995). The experimental design also had in-line pH monitoring capabilities so that proton evolution could be monitored. The experiments were conducted with 10 mg/L Pb (48.3 μM) with an ionic strength of 0.01 mol/L in $NaNO_3$ at pH 5.5 and also with 0.01 mol/L KNO_3 with all other conditions being the same. Under these conditions, the experiments were undersaturated with respect to lead hydroxides and carbonates (Fig. 2). The experimental effluent solution was analyzed using

aqueous spectroscopic methods (atomic adsorption, spectroscopy and inductively coupled plasma spectroscopy) and the reacted solids were analyzed using microscopy (field emission scanning electron microscopy), bulk surface chemical spectroscopy (energy dispersive spectroscopy), and surface sensitive spectroscopy (X-ray photoelectron spectroscopy).

This Pb concentration was chosen to (1) allow for the oxides to sorb significant amounts of Pb, (2) limit any analytical difficulties and errors that arise when working with very low concentrations near detection limits, and (3) reflect the Pb exposure of soil minerals at highly contaminated sites. Extremely wide ranges are reported for the Pb content values for both uncontaminated and contaminated soils (see Davies, 1995; Chlopecka and Adriano, 1997), and soil solution values are rarely reported. Tampouris et al. (2001) studied an acidic (pH 5.6, similar to this study) soil that was contaminated from mining activities with approximately 16000 mg Pb/kg dry soil. Gregson and Alloway, (1984) extracted the soil solution from several contaminated soils and found soil solution values ranged from 4 mg/L to 112 mg/L.

The Mn-oxides we studied are birnessite, pyrolusite, and cryptomelane. Birnessite (in our synthetic runs, $K_4Mn_{14}O_{27} \cdot 9H_2O$) is the most common Mn oxide in soils and is generally found as discrete soil nodules, dessert varnishes, and ocean nodules (Taylor et al., 1964; Burns and Burns, 1979; McKenzie, 1989; Dixon and Skinner, 1992; Post, 1992). All known natural birnessite samples are either poorly crystalline or consist of minute crystals; thus these materials have not been extensively characterized (Post, 1992). Birnessite does have a layer structure with both Mn^{3+} and Mn^{4+} (Post, 1992). Pyrolusite (β-MnO_2) is the most stable form of MnO_2, but it is rare in soils because even small amounts of foreign ions prevent the formation of pyrolusite (McKenzie, 1989). It is generally found in low temperature hydrothermal deposits and as alteration products of other Mn-oxide minerals (Post, 1992). Pyrolusite is a framework structure containing tunnels (1×1 octahedra) formed by edge-linked Mn(IV)O_6 octahedra sharing corners with neighboring chains. Cryptomelane ($K_x(Mn^{4+}Mn^{3+})_8O_{16}$($x \approx 1.3$–1.5) or generally α-MnO_2) is part of the hollandite group (McKenzie, 1989; Post, 1992), and its structure consists of double chains of edge-sharing Mn-O octahedra that share corners with each other to form a framework structure with 2×2 (octahedral on edge) tunnels (Post, 1992). The tunnels are partially filled with large mono or divalent cations and sometimes water molecules. The charges on the tunnel cations are balanced by substitution of Mn^{2+} or Mn^{3+} on the octahedral site. The minerals within the hollandite group are defined on the basis of the principal type of tunnel cations as follows: hollandite (Ba), coronadite (Pb), and cryptomelane (K) (McKenzie, 1989; Post, 1992). McKenzie (1989) describes this group of minerals as "reasonably common" in soils.

Iron oxides were also tested in this study because Pb sorption is often attributed to Fe-oxides in soils as well as or rather than Mn-oxides. The Fe-oxides we studied are goethite, hematite, ferrihydrite, and akaganéite. These solids were chosen because they are either very common phases in nature or they are isostructural with one of the Mn-oxide phases we planned to study. Goethite (α-FeOOH) is the most common and thermodynamically stable iron oxide in soils. Goethite has double rows of $FeO_3(OH)_3$ octahedra, which share edges and corners to form 2×1 octahedra "tunnels" (only large enough to accommodate the passage of protons) partially bonded by hydrogen bonds (Schwertmann and Cornell, 1991; Sparks, 1995; Cornell and Schwertmann, 1996). Hematite is the second most common iron oxide in soils (Sparks, 1995). Hematite (α-Fe_2O_3) consists of FeO_6 octahedra connected by edge- and face-sharing (which causes distortion in the cation sublattice from ideal packing) (Sparks, 1995; Cornell and Schwertmann, 1996). Ferrihydrite is a poorly ordered Fe^{3+} oxide that has short range ordering and is prevalent in surface environments where it is often a precursor for other Fe-oxides (Schwertmann and Taylor, 1989; Cornell and Schwertmann, 1996). Akaganéite (β-FeOOH) is isostructural with cryptomelane (Cornell and Schwertmann, 1996).

2. MATERIAL AND METHODS

2.1. Reagents

All chemicals used in the experiments were reagent grade or better. Trace metal grade or standardized acids and bases were used for pH adjustments. High-purity distilled, deionized water from a Millipore Synthesis A10 water system (18.2 MΩ, $<$8ppb total organic carbon (TOC), UV light treated, ultrafiltration membrane, 0.2 μm filtered) was used to make all solutions. All glass and plastic ware was acid washed using a 0.1 mol/L nitric acid bath; if any dishes appeared to be stained by Mn or Fe oxides, they were soaked in a 0.05 mol/L oxalic acid bath. The dishes were then soaked in distilled, deionized water.

2.2. Minerals

Both natural and synthetic Mn and Fe-oxide mineral samples were used in this study. For convenience, we have used the corresponding mineral name even for the synthetically prepared oxides (e.g., synthetic cryptomelane instead of α-MnO_2). The identities of the solids were verified using X-ray powder diffraction (Table 1 and Figs. 3 and 4). The samples were further characterized by low-voltage field-emission scanning electron microscopy (FE-SEM), energy dispersive spectroscopy (EDS), BET N_2 adsorption specific surface area analysis, and isoelectric point (IEP) measurements.

2.2.1. Synthetics

The synthetic solids used in this study are listed in Table 1 along with their BET N_2 surface area. Synthetic Mn-oxides and Fe-oxides were made using methods found in McKenzie (1971) and Schwertmann and Cornell (1991), respectively. When necessary, the "recipes" were scaled back (i.e., less sample was prepared) for ease of preparation in our laboratory. All the solids were washed with trace metal clean dialysis tubing (Fisherbrand, 32mm, 10,000 MWCO) until the conductivity of the soaking water matched that of distilled, deionized water; once washed, the samples were freeze dried. A detailed account of the synthesis of all Mn- and Fe-oxides used in this study can be found in O'Reilly (2002).

2.2.2. Natural solids

Table 1 also lists the natural solids used in this study. While synthesizing solids yields a fine-grained mineral form suited toward our flow experiments (also a grain size often found in soils and sediments), most of the natural solids needed to be reduced in size to be more like the synthetic samples. Large mineral fragments were crushed to $<$0.5 mm in a percussion mortar and then were wet-ground in distilled, deionized water for 10 min using a McCrone Micronizing Mill (a vibrating rod mill). This method is the best way of reducing particle size while avoiding many of the negative effects associated with more aggressive, traditional grinding methods (Buhrke et al., 1998). The resulting BET N_2 surface area is given in Table 1.

Table 1. Summary of chemical structural properties of the Mn and Fe-oxides used in this study.

Mineral	Abbreviation Used in Text and Figures	General Formula	Lending Institution Or Synthesis Reference	Origin or Synthesis Method	Structure	BET, N_2 Surface Area m^2/g	Matching JCPDS File(s)
Mn-oxides							
Natural							
Cryptomelane	Cr1	$K_{1.3–1.5}(Mn^{4+}Mn^{3+})_8O_{16}$[a]	NMNH[e]	Sitpar Mn Mine, Chindara, India	2 × 2 tunnel	5.3	44–1386,
	Cr2		VPI[f]	Unknown		14.9	44–1386, 42–1348
Pyrolusite	PY8	MnO_2[a]	VPI	Unknown	1 × 1 tunnel	7.9	(Weaver, 2001)
Synthetic							
Birnessite		$K_4Mn_{14}O_{27} \cdot 9H_2O$[b]	(McKenzie, 1971)	Heated reduction of $KMnO_4$ with HCl	layer	35.4	23–1239
Cryptomelane, α-MnO_2		$K_{1.3–1.5}(Mn^{4+}Mn^{3+})_8O_{16}$[a]	(McKenzie, 1971)	Convert birnessite by ignition	2 × 2 tunnel	25.7	42–1348, 44–1386
Pyrolusite, β-MnO_2		MnO_2[a]	(McKenzie, 1971)	Ignition of evaporated manganous nitrate	1 × 1 tunnel	0.15	81–2261, 72–1984, 24–0735
Fe-oxides							
Natural							
Hematite	M2258	α-Fe_2O_3	VPI	Clinton, NY		8.2	87–1165
	D61		VP1	Rio Marina Mine, Rio Marina, Isula D'Elba, Italy		4.6	87–1165
Goethite	Fe11	α-FeOOH	Private donor	Pikes peak batholith		4.0	29–0713
Synthetic							
Hematite, α-Fe_2O_3		α-Fe_2O_3	(Schwertmann and Cornell, 1991	Method 1, forced hydrolysis of Fe(III) salt		42.5	87–1165
Goethite, α-FeOOH		α-FeOOH	(Schwertmann and Cornell, 1991)	Fe(III) alkaline system, heated		76.3	(Waltham and Eick, 2002)
Ferrihydrite (6-line)		$Fe_5OH_8 \cdot 4H_2O$[c]	(Schwertmann and Cornell, 1991)	Hydrolysis of acidic Fe(III) solution		193.3	29–0712
Akaganéite, β-FeOOH		$FeO_{0.8}(OH)_{1.2}Cl_{0.2}$[d]	(Schwertmann and Cornell, 1991)	Hydrolysis of acidic $FeCl_3$		116.4	34–1266,42–1315

[a] (Post, 1992)
[b] (Burns, 1976) assuming equal substitution of K for Na given in original formula.
[c] (Schwertmann and Cornell, 1991)
[d] (webmineral.com, 2002)
[e] NMNH- National Museum of Natural History of the Smithsonian Institution
[f] VPI- Virginia Polytechnic Institute and State University, Department of Geological Sciences Museum

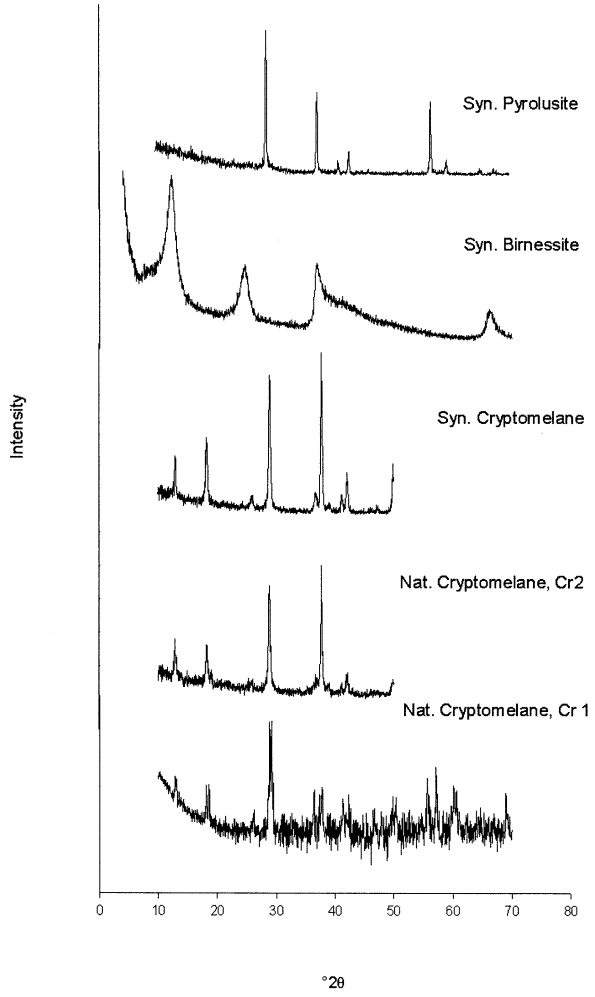

Fig. 3. Cu K_α XRD patterns of the Mn-oxides prepared for this study. The natural cryptomelane, Cr 1 spectra has been background subtracted and smoothed as the pattern was taken before the diffractometer was optimally adjusted.

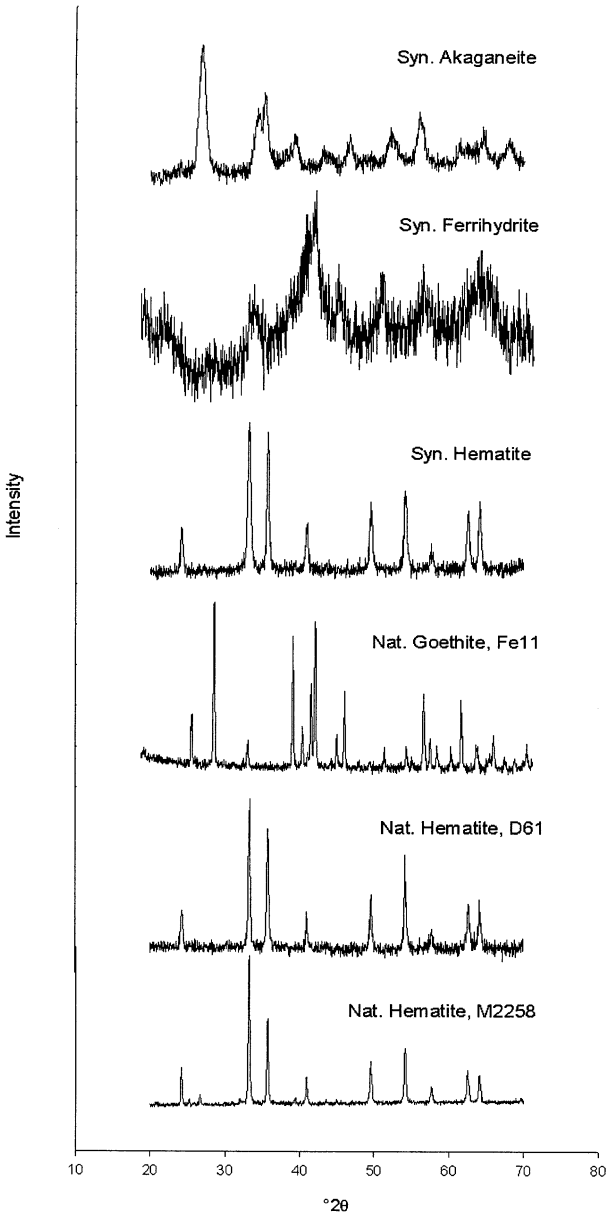

Fig. 4. Cu K_α XRD patterns of the Fe-oxides prepared for this study.

2.3. Techniques

2.3.1. Surface area analysis

Specific surface area was measured using the BET N_2 adsorption method using a Nova 1200 high-speed surface area and pore analyzer manufactured by Quantachrome. Single and 5-point BET measurements were made. Sorption data is normalized according to the 5-point measurement, however the two measurements agreed well. Samples were vacuum degassed overnight at 40 °C to minimize the possibility of phase changes during high temperature degassing. To get an approximation of internal surface area, the ethylene glycol monoethyl ether (EGME) method (Carter et al., 1965) was used to measure the total specific surface area for the solids most likely to exhibit the most internal surface area (the synthetic birnessite and cryptomelane).

2.3.2. X-ray diffraction (XRD)

XRD was used to identify the natural and synthesized solids. Powder measurements were taken using a Scintag XDS 2000 X-ray powder diffractometer. Powder mounts were prepared directly in the sample holders or on zero background plates depending on the amount of sample. A CuKα radiation source was used and the window on the detector was adjusted to minimize the contributions of fluorescence. Continuous scans of reacted solids on filter paper and synthetic birnessite were run from 4 to 70° 2θ. Reacted solids were scanned at 4°/min; because of the poorly crystalline nature of birnessite, it was scanned at 1°/min. All other scans were made from 10 to 70° 2θ (or 50° 2θ in the case of two of the cryptomelane samples that were x-rayed again after window adjustment) at a scan rate of 4°/min. The samples were spun to minimize the possibility of any preferential orientation in the mounts.

2.3.3. Atomic absorption spectroscopy (AA)

Analysis of aqueous Pb was performed using a Buck Scientific 200-A AA. Four standard dilutions of a purchased 1,000 ppm Pb AA standard reference solution (Fisher chemical) ranging from 0.8 to 12 ppm Pb were analyzed to produce a calibration curve of absorbance versus concentration. The standards were made in the identical matrix used in each of the runs. The standards were measured in triplicate at the beginning and end of each run; average values were used to plot the

calibration curve. The AA was adjusted to a slitwidth of 7Å, a wavelength of approximately 283.3 nm, and a 5.0 mA lamp current using an air-acetylene flame. The sensitivity for this method is reported as being approximately 0.2 mg/L (ppm) (Welz and Sperling, 1999). All the measurements were taken in triplicate and averaged before being converted to concentration. The AA was operated on integration mode to eliminate the measure of errors due to random noise; this method averages the signal taken over 7 s before reporting a reading (Buck Scientific, 1992). The AA was rinsed and rezeroed between every sample to avoid contamination and drift.

2.3.4. Inductively coupled plasma atomic emission spectrometry (ICP-AES)

Analysis of KNO_3 matrix samples for Pb and Mn or Fe (for Mn and Fe-solids respectively) was performed on a Spectro Analytical Instruments SpectroFlame (type FTMA85D) ICP. The ICP was used because of its low detection limits for Mn and its ability to measure multiple elements at once. The measurements were performed at wavelengths of 168.220 nm for Pb, 257.610 nm for Mn, and 259.940 nm for Fe. Measurements were taken from the sample in triplicate. Lead analysis on the ICP was found to correspond well with AA analysis of Pb for the same samples. The ICP generally detects Pb in the analytical range of 0.05–10,000 ppm, Mn from 0.001–5000 ppm, and Fe from 0.002–10,000 ppm.

2.3.5. Field emission scanning electron microscopy (FE-SEM) and energy dispersive spectroscopy (EDS)

Low voltage FE-SEM imaging and EDS analyses were performed with a LEO 1550 FE-SEM with Kevex EDS detector. Some unreacted Mn-oxides and many of the Fe-oxides (especially less crystalline samples) were conductively coated for ease in imaging; however, many samples were not coated at all. Experience in our laboratory has shown that when operating the FE-SEM at low voltage (<5 kV) and using the "SE^I" detector, excellent lateral resolution of <5nm can be achieved (Weaver, 2001). The backscatter detector was also used to check for Pb precipitates on the surfaces of the oxides. The beam was often adjusted in one area, moved, and then an image was quickly taken to avoid beam damage to any possible precipitates. EDS analysis was taken at lower magnifications and higher voltages ($\approx$20 kV).

2.3.6. X-ray photoelectron spectroscopy (XPS)

Selected samples were analyzed with a Perkin-Elmer 5400 using an Al X-ray source. Survey spectra of selected solids were collected with a pass energy of 44.75 eV from 0 to 1000 eV binding energies for 5 min. High-energy resolution scans of Mn2*p* and Pb4*f* peaks were collected from 630–670 and 130–150 eV binding energies, respectively using a pass energy of 17.90 eV. The Pb/Mn atomic ratio was calculated using standard sensitivity factors obtained from standards measured in the 5400 hemispherical electron energy analyzer. The analysis area of each sample was approximately 1×3 mm.

2.3.7. Zeta potential

A Malvern Instruments ZetaSizer 3,000 HSa was used to measure the electrophoretic mobility via laser Doppler velocimetry. The zetasizer estimates the zeta potential from the electrophoretic mobility using the Smolouchowski equation. The isoelectric point (IEP), the point at which the electrokinetic potential equals zero (Kosmulski, 2001), was determined by plotting the average of at least three zeta potential measurements each at a minimum of six different pH values for solids that were hydrated and sonified in the background matrix (0.01 mol/L $NaNO_3$ or 0.01 mol/L KNO_3) for at least 4 d. After initial equilibration, 25 mL of the hydrated mineral suspension (0.25 mg/L except for the ferrihydrite which was run at 0.125 mg/L) was added to plastic centrifuge tubes and then pH adjusted over at least 6 d. The pH was adjusted by microliter additions of 0.1 mol/L HNO_3 and 0.1 mol/L NaOH or KOH (corresponding to $NaNO_3$ and KNO_3 matrices respectively). The final pH was measured at the same time that an aliquot of the suspension was being analyzed in the zetasizer. Since the exact shape of the plot cannot be predicted, this method does not allow for extrapolation; thus, solids with a very low IEP such as birnessite can only be estimated to be below a certain pH.

2.4. Flow-Through Experimental System

Lead sorption studies were conducted using a flow-through reactor so that chemical steady state conditions were maintained during the experiments (Rimstidt and Newcomb, 1993; Sparks, 1995). The experiments were initially run in duplicate; after acquiring a third pump, all the experiments were run in triplicate. The influent Pb concentration was 10 ppm (48.3 μM) adjusted to an ionic strength of 0.01 mol/L with $NaNO_3$ for one set of experiments and KNO_3 for another set of experiments. The pH of the influent solution was preadjusted to pH 5.5; under these conditions, as shown in Figure 2, the system was undersaturated with respect to known lead oxides and hydroxy carbonates. Tygon tubing was used everywhere except for the tubing link that is inserted in the pressure plate of the cassette pump. The tubing link was made of Manostat Manosil tubing with cuffs to ensure uniform placement and tension in the pumps. The pumps were Manostat Junior or Jimmy cassette pumps (model 42-510-000). To minimize flow variations, a brand new tubing link was used for every experiment. Since Pb is known to sorb onto the walls of containers, each link was pretreated with influent Pb solution (pH and ionic strength adjusted) for at least 4 h and then rinsed with matrix solution before its use. The influent bottles and Tygon tubing were reused for each experiment, but the system was flushed with the new matrix solution before starting runs in the new matrix.

The reactors consisted of 25 mm Swin-Lok polycarbonate filter holders (Corning) with the sorbent wet packed onto a 0.2μ Pall Gelman Supor membrane filter paper (see next section for choice of filters). All of the solids in powder form were prehydrated in the appropriate matrix solution overnight, sonified, and adjusted to pH 5.5 over a minimum of 5 d before being loaded onto the reactor. The filter paper was placed into the reactor (filter holder) and rinsed two times with 2 mL of pH-adjusted matrix solution by pipetting the solution into the barrel of a syringe attached to the filter holder on a vacuum flask that was connected to an aspirator run at $\leq$5 kPa. Then the reactor was wet loaded with the appropriate amount of the solid suspension to yield 0.5 m^2 specific surface area of solid except for synthetic pyrolusite, which was run at 0.06 m^2 due to its very low surface area. The solid suspension was rinsed into the reactor three times with 2 mL of pH-adjusted matrix solution. In-line pH measurements were made using a pH cell made of polycarbonate holding an Accumet (model 13–620–181) rugged bulb pH electrode. The pH electrode was wired to a Prober pH 8 datalogger (Erhlich Industrial Development Corporation, E.I.D.) and connected to a computer, which recorded pH readings every two minutes.

Samples were collected by fraction collectors every 20 min into tubes that were previously acid washed, soaked in distilled, deionized water, and preacidified with trace metal grade HNO_3. The tubes were weighed and labeled before the start of the experiment and then were reweighed at the end of the experiment to more accurately determine the total amount of solution passed through the reactors and to closely monitor the flow rates. The collected fluid samples were refrigerated until analyzed by AA or ICP.

Experiments were deemed acceptable if the flow rate was $>$0.40 or $<$0.75 mL/min; the average flow rate was 0.55 mL/min. Within this flow range, flow rate did not correlate to Pb sorption. Runs with flow rates higher than 0.75 mL/min did occasionally show correlation of Pb sorption amounts with flow rate, this was probably due to channelized flow in the packed reactors. The results of these runs were not used. Other runs were eliminated due to leaks in the system or other mechanical problems.

Different types of "blank" experiments were run to better understand our system. A set of blank experiments was conducted (1) without mineral, (2) without Pb in the influent solution, and (3) without both the mineral and the Pb in the influent solution. The set of blanks run without Pb influent solution were run only with the cryptomelane mineral solid in KNO_3 to determine the amount of Mn release from the cryptomelane samples. All blank runs were run through the same physical apparatus including filter paper and the appropriate, pH adjusted background electrolyte.

2.4.1. Choice of membrane filter papers

The Pall Gelman Supor membrane filter paper, a polyethersulfone membrane, was chosen after testing several filter papers of varying composition and brands for Pb sorption. While developing our experimental methodology, it was discovered that Pb was being sorbed by the MCE membranes (comprised of a mixture of cellulose acetate and cellulose nitrate) that had been used initially. Teflon and polycarbonate filter papers were two other compositions that were tested. The hydrophobic nature of Teflon filters makes them more difficult to work with in these types of experiments. However, suitable results were also found with polycarbonate filter papers. The Supor filter papers were ultimately chosen after discussions with the company regarding manufacturing processes; we were also concerned about the filters introducing metals into our experiments. Specific experimental results obtained from the filters we used are given in the Data Analysis and Errors and pH sections below.

2.5. Data Analysis and Errors

A sample of the influent solution was collected from the flow lines before it entered the reactor and measured by AA or ICP using the same protocol as for the reactor output described above. The amount of Pb sorbed onto the sample was determined by difference. The amount of Pb sorption was normalized to the BET surface area of the solids to give units of μmol of Pb sorbed per m^2 of solid. Because the flow rates from all runs were similar but not exactly the same (see section 2.4. above), we did not want to compare the amount of Pb sorbed after 5 h (the end of the experiment); instead we decided to pick the highest volume of solution that passed through the reactors from all of the acceptable runs. Therefore, the total amount of Pb sorbed after an average of 119.8 mL of solution was passed through the reactors was used to compare the amount of Pb sorbed to the different solids. Overall, this method allows for the direct comparison of the many different solids examined in this study.

Blank experiments were run to determine a typical amount of Pb sorbed by the experimental system when a Pb-containing influent solution was passed through the system in the absence of a mineral powder; this is referred to as a mineral-blank run. The result of four repeat runs were that 3.24 ± 0.89 mg/L total Pb was sorbed by the experimental system after approximately 119.8 mL of solution had passed through the reactors. We chose the best filter papers available for our experiments (see section 2.4.1. above), but obviously they are not ideal and, of course, their impurities, Pb uptake abilities, and surface area can be variable. This variability makes it impossible to adjust or correct the mineral Pb uptake results due to the presence of the filter, but in all runs the mineral remained by far the dominant uptake material except for synthetic akaganéite in the $NaNO_3$ electrolyte. In this latter case, the mineral sorption was so minimal (see section 3.3. below) that the filter sorbed about as much Pb as the akaganéite itself.

The possible sources of error in our study are analysis errors (AA and ICP), variations in the filter paper sorbates and leachates, variations in flow due to the packing of the different solid particles or the pump, BET measurement errors (since used to normalize our data), possible sample heterogeneity, and possible differences in the surface area of the aliquot of sample used in the reactor versus that measured in the BET.

3. RESULTS AND DISCUSSION

3.1. IEP

IEP estimates for the solids examined in this study are shown in Table 2. Where extrapolation would be needed due to the nature of the sample, or due to the limited pH range of some of the samples, greater than or less than symbols are used to indicate the approximate IEP value. As can be found in the literature, the IEP values (as well as point of zero charge, pzc, and similar values) of the solids range widely. Cornell and Schwertmann (1996) and references therein show IEP values ranging from 7.4–9.5 for goethite, 6.4–7.3 for akaganéite, and 7.0–9.4 for hematite. The authors note that the IEP is very sensitive to impurities, thus we would expect that natural samples could have very different IEP values than synthetic samples. The extensive review by Kosmulski (2001) and references therein show even greater IEP ranges for goethite (and synthetic α-FeOOH) of approximately 5.6–9.5, hematite from 3 to 9.5, and ferrihydrite from 7.2–9.8 (see Kosmulsk, 2001 for more details and specific references). Mn-oxide IEP values also range widely; pyrolusite ranges from 4.4 to 7.3, and cryptomelane only had one IEP value reported at ~4.6, but other methods reported values ranging from 3 to 5.4 (Kosmulski, 2001 and references therein). Measuring the zero charge conditions of birnessite is very difficult due to numerous problems with these measurements at low pH (Healy et al., 1966; Murray, 1974; McKenzie, 1981). Most values are only obtained from methods that allow somewhat reliable extrapolation and are not actually directly measured. Regardless, methods other than IEP determination show a range of values for the pH at zero charge conditions for birnessite ranging from 1.5 to 3.6 (see Kosmulski, 2001).

Table 2. Estimated Isoelectric Points (IEP) of the Mn and Fe-oxy(hydr)oxides used in this study.

	0.01 M Matrix	
Solids	$NaNO_3$	KNO_3
Fe-oxy(hydr)oxides		
Nat. Hematite, M2258	<4.0	<4.0
Nat. Hematite, D61	6.8	6.8
Nat. Goethite, Fe11	7.0	6.7
Syn. Akaganéite	6.6	≥6.7
Syn. Hematite	7.3	7.2
Syn. Goethite[a]	9.2	Not measured
Syn. Ferrihydrite	6.8	6.9
Mn-oxides		
Nat. Pyrolusite, Py8	4.9	6.5
Nat. Cryptomelane, Cr2	6.2	≥6.8
Nat. Cryptomelane, Cr1	4.3	6.7
Syn. Cryptomelane	≤6.0	6.2
Syn. Pyrolusite	≤4.3	6.5
Syn. Birnessite	<2.0	<2.0

[a] Luxton, T. and M. Eick (private communication).

The limited information on Mn-oxides in common compilations and textbooks generally report that most Mn-oxides have IEP or pzc values below that of most Fe-oxides (i.e., Sparks, 1995; Zelazny et al., 1996; Langmuir, 1997). Under the conditions of our study, Mn-oxides did generally have lower IEP values in $NaNO_3$ solutions than Fe-oxy(hydr)oxides did. However, the same observation does not hold for the values measured in KNO_3 background electrolyte solutions. Fe-oxide measurements are virtually identical in either matrix, but the IEP of the Mn-oxides in the KNO_3 matrix are most often significantly greater than in the $NaNO_3$ background electrolyte. At pH 5.5 (the pH of the sorption experiments reported in this study), Fe-oxides, with the exception of one natural hematite sample (M2258), would have a net positive charge on the surface. The Mn-oxides in KNO_3 also have a net positive charge on the surface with the exception of birnessite. In $NaNO_3$, all the Mn-oxides, except one of the natural cryptomelane samples (Cr 2) and possibly synthetic cryptomelane, have a net negative charge. If electrostatics were to play a

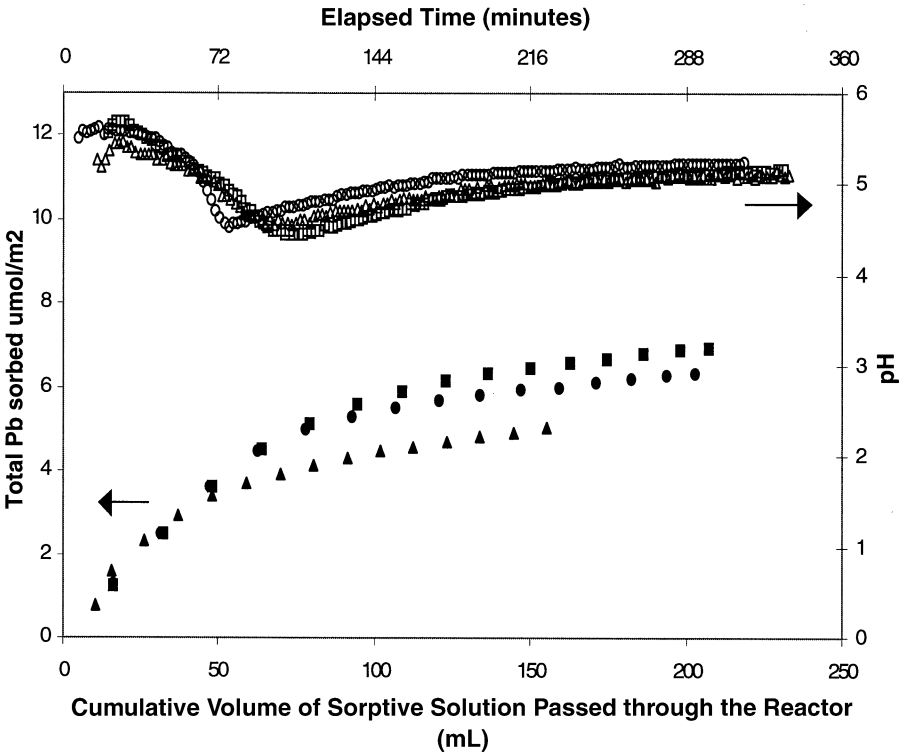

Fig. 5. Lead sorbed on synthetic cryptomelane in $NaNO_3$ background electrolyte and reaction pH. The reaction pH is plotted versus elapsed time using open symbols, and the Pb sorption is plotted in terms of the total amount of Pb sorbed normalized to the surface area of the solid using closed symbols. The plot shows triplicate runs.

major role in the reaction of aqueous Pb with the oxides, then sorption on the solids would follow the order Mn-oxide $>$Fe-oxides in $NaNO_3$ (with noted exceptions) and Fe-oxides $\approx$ Mn-oxides in KNO_3. Pb sorption should be greater in the $NaNO_3$ matrix than in the KNO_3 matrix.

Interestingly, the shift in the IEP of the Mn-oxides in the presence of K versus Na may indicate that K is interacting preferentially or differently with these surfaces. Other studies have come to similar or supportive conclusions (Healy et al., 1966; Yousef et al., 1971; Murray, 1974; Balistrieri and Murray 1982). For example, Yousef et al. (1971) studied β-MnO_2 and found that changing the cation of the supporting electrolyte by using 10^{-3} M KNO_3 vs. $NaNO_3$ produced a slightly less negative ξ potential. This bears further consideration when the sorption study results are discussed below.

3.2. pH

Figure 5 shows a fairly typical pH variation and Pb uptake response for a triplicate set of full experimental runs involving synthetic cryptomelane in $NaNO_3$ background electrolyte. This solid is one of the more reactive ones and thus the initial change in pH is relatively pronounced. Most of the general trends in the pH with time follow that shown in this plot with the pH usually dropping early in the experiment and then recovering back to the influent level after the Pb sorption levels off. Unfortunately, the variability of H evolved in many of our blank experiments (ultimately due to the variability of the filter paper reacting with the matrix solution or Pb influent solution) makes it impossible to calculate the amount of H evolved relative to the amount of Pb sorbed in the actual experimental runs or to calculate a mass balance for Pb, Mn, and H.

3.3. Lead Sorption on Manganese and Iron Oxides

Figure 6 shows the data for the total Pb sorption to the Mn- and Fe-oxides in both $NaNO_3$ and KNO_3 background electrolytes. The data is normalized to the BET surface area of the mineral sample in that run. This figure clearly shows that some Mn-oxides sorb significantly more Pb than Fe-oxides per surface area. Synthetic birnessite removes almost an order of magnitude more Pb from solution than the Fe-oxides. However, the natural pyrolusite Py8 and the natural cryptomelanes, Cr1 and especially Cr 2, remove a similar amount of Pb from solution as many of the natural and synthetic Fe-oxides.

All the Fe-oxides run in this study sorb fairly similar amounts of Pb once normalized to BET N_2 surface area. Also, there are not any clear trends between the synthetic and natural Fe-oxides. However, it is interesting to note that synthetic akaganéite, especially in the $NaNO_3$ matrix, has a particularly low affinity for Pb.

The synthetic Mn-oxides do have higher affinities for Pb than the natural Mn-oxides. The synthetic and natural pyrolusites have particularly striking differences whereas the cryptomelanes are not nearly so different. The general order of sorption in KNO_3 is Nat. cryptomelane, Cr2 $\approx$ Nat. pyrolusite, Py8 $<$ Nat. cryptomelane, Cr1 $<$Syn. cryptomelane $\approx$ Syn. pyrolusite $<$ Syn. birnessite. The order is slightly different in

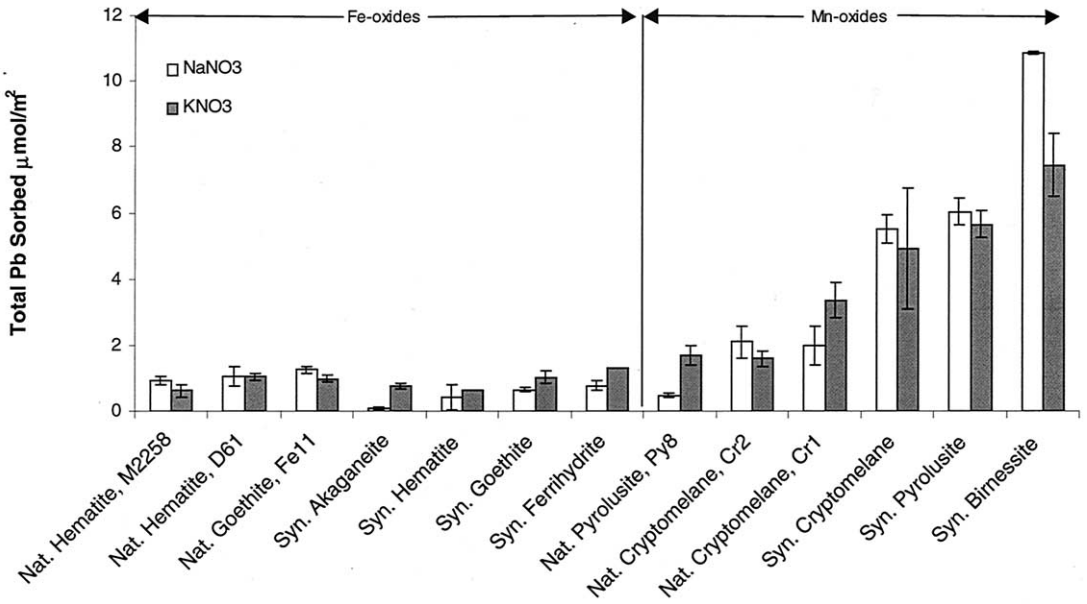

Fig. 6. Total average Pb sorption in umol/m^2 (normalized to the BET surface area of the solid) after approximately 119.8mL of solution has passed through each reactor. The error bars denote plus or minus the standard error of the mean of duplicate and triplicate runs. Studies conducted in $NaNO_3$ background electrolyte are displayed using white bars while studies conducted in KNO_3 background electrolyte are denoted by gray bars. The Fe-oxides are listed to the left, and the Mn-oxides are listed on the right of the figure.

the $NaNO_3$ background electrolyte with Nat. pyrolusite, Py8 $<$ Nat. cryptomelane, Cr2 $\approx$ Nat. cryptomelane, Cr1 $\ll$ Syn. cryptomelane $\approx$ Syn. pyrolusite $\ll$ Syn. birnessite.

Synthetic akaganéite, goethite, and ferrihydrite show differences beyond experimental error in Pb sorption in different electrolyte solutions. These three synthetic Fe-oxide solids all had lower affinities for Pb in the $NaNO_3$ bathing solution. For the Mn-oxides, Nat. pyrolusite Py8, Nat. cryptomelane Cr1, and Syn. birnessite displayed differences beyond experimental error in Pb sorption between the two electrolytes. Natural pyrolusite and Nat. cryptomelane Cr1 results indicated increased Pb sorption in a KNO_3 solution environment whereas the Syn. birnessite reacted more strongly with Pb in the presence of the $NaNO_3$ electrolyte.

Comparing the sorption trends in Figure 6 to the IEP data shown in Table 2, we see that a few of the points do show agreement between the IEP magnitude and the amount of sorption; for example, the very high affinity of the synthetic birnessite for Pb could be rationalized by its very low IEP (noting that a lower IEP would mean a more negative surface and therefore more attraction for the Pb^{2+} ion). However, the overall IEP trends do not match up with the sorption affinity series given above. Additionally, the Nat. pyrolusite Py8 and the Nat. cryptomelane Cr1 electrolyte sorption trends in the two electrolytes do not coordinate with the IEP values. Both the Py8 and Cr1 show increased sorption in the KNO_3 electrolyte despite the solid having higher IEP values in the potassium electrolyte. However, many studies note that the operative mechanism of Pb removal from solution by Mn-oxides is specific (inner-sphere) adsorption (Manceau et al., 1997; Morin et al., 1999; Ostergren et al., 1999; Matocha et al., 2001; Manceau et al., 2002).

3.4. FE-SEM

Low voltage, nanometer resolution FE-SEM images are shown in Figures 7 and 8 of the synthetic cryptomelane and synthetic birnessite samples, respectively, as examples. The morphology of the synthetic cryptomelane sample exhibits hexagonal platelets, and the morphology of the synthetic K-birnessite sample resembles that of a barite rose. Yang and Wang (2002) showed a fairly similar SEM image of a randomly stacked synthetic birnessite. However, our XRD data clearly showed a peak at 7.20 Å, indicating that we do not have randomly stacked birnessite. Matocha et al. (2001) used the same synthesis method as used in this study to make K-birnessite and regarded their solid as being structurally similar to hexagonal birnessite.

Only one image is shown for the synthetic birnessite and cryptomelane samples because the before and after images were virtually identical; we did not observe any microprecipitates or dissolution features on the reacted solids. Manceau et al. (1992) claimed that Pb multinuclear surface complexes were forming on birnessite; however, Manceau et al. (2002) did not see any evidence of surface precipitation when they studied Pb and other metals reacting with various synthetic birnessite samples using polarized and extended X-ray absorption fine structure (EXAFS) spectroscopy. Matocha et al. (2001), using EXAFS, also did not discover surface precipitates on synthetic birnessite or manganite.

Figures 9 and 10 are FE-SEM images of unreacted natural cryptomelane Cr1 and natural cryptomelane Cr2 samples respectively. Once normalized to surface area, one might expect that these solids would sorb more than the synthetic cryptomelane, which has flat hexagonal platelets, due to their increased microtopography (e.g., Junta and Hochella, 1994).

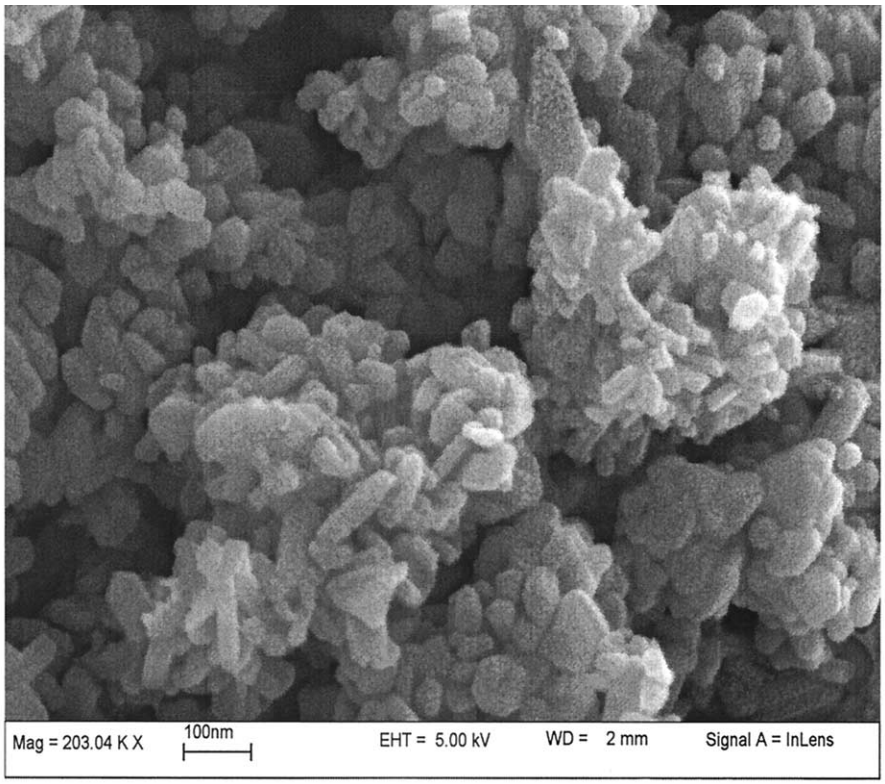

Fig. 7. High-resolution FE-SEM image of synthetic cryptomelane. Note the scale bar denotes 100 nm. The image shows that the crystal morphology is dominated by hexagonal platelets; the minute bumps on the plate surfaces are due to the gold conductive coating applied to the unreacted sample before SEM imaging.

However, as seen in Figure 6, the opposite is true. In this case, the microtopography may not be playing a major role in determining the sorption efficiencies of the solids. One overriding factor may be that different crystallographic faces are exposed in the natural, micronized cryptomelane samples versus the synthetic, unground samples.

3.5. EDS

Figure 11 shows the EDS spectrum of the natural cryptomelane Cr1 before reaction with Pb. This shows that Cr1 does have some Si, Al, Na, and Ba (the EDS for Cr2 is very similar). It is not surprising to see some Ba in the natural sample because in nature the hollandite group, of which cryptomelane is a member, is generally composed of solid solutions rather than pure end members; hollandite itself has primarily Ba in its tunnels. Na is also substituting for K in the tunnels. Al and Si are also present so it is likely that we are seeing some additional phases or compositional impurities that were not detected in the X-ray diffraction data. Any of these impurities, as mentioned earlier, could affect the IEP of the solid and possibly the available reactive sites on the solid. These compositional impurities may account, in part, for the differences in the sorption of the natural versus the synthetic Mn-oxides.

3.6. XPS

Figure 12 shows the XPS survey scan of unreacted synthetic birnessite that was equilibrated in 0.01 mol/L KNO_3 matrix solution before being run in a Pb sorption experiment. Also shown are synthetic birnessite, natural cryptomelane Cr1, and synthetic cryptomelane after being run in a Pb sorption experiment using the $NaNO_3$ background electrolyte. As expected, the unreacted synthetic birnessite sample shows K (due to synthesis and background electrolyte composition) but no Pb in the XPS spectrum. Sodium is present in the near-surface region of the reacted birnessite and cryptomelane run in $NaNO_3$ electrolyte; however, K-birnessite was originally synthesized for these experiments and cryptomelane has K as the major tunnel cation in its structure so a K peak would be expected in the XPS spectra. This clearly indicates that the K has exchanged with the Na in the background elecrolyte, at least as far as near-surface analysis is concerned in these samples.

Table 3 compares the solution data results from the $NaNO_3$–background flow study to the Pb surface enrichment information from the XPS high energy resolution scans (data not shown). The table displays the Pb/Mn atomic ratio along with the total Pb uptake after sorption runs for synthetic cryptomelane, natural cryptomelane Cr1, natural cryptomelane Cr2 and synthetic birnessite. Looking at the Pb/Mn ratios, synthetic cryptomelane has the most Pb enriched at the surface, followed by natural cryptomelane Cr1, and then finally the natural cryptomelane Cr2 and synthetic birnessite having the least amount of Pb enriched at the surface. Interestingly, synthetic birnessite removed the most Pb from solution (referring to our aqueous flow-studies). Because XPS is surface sensitive, it cannot "see" the interlayer of the birnessite structure except for those few

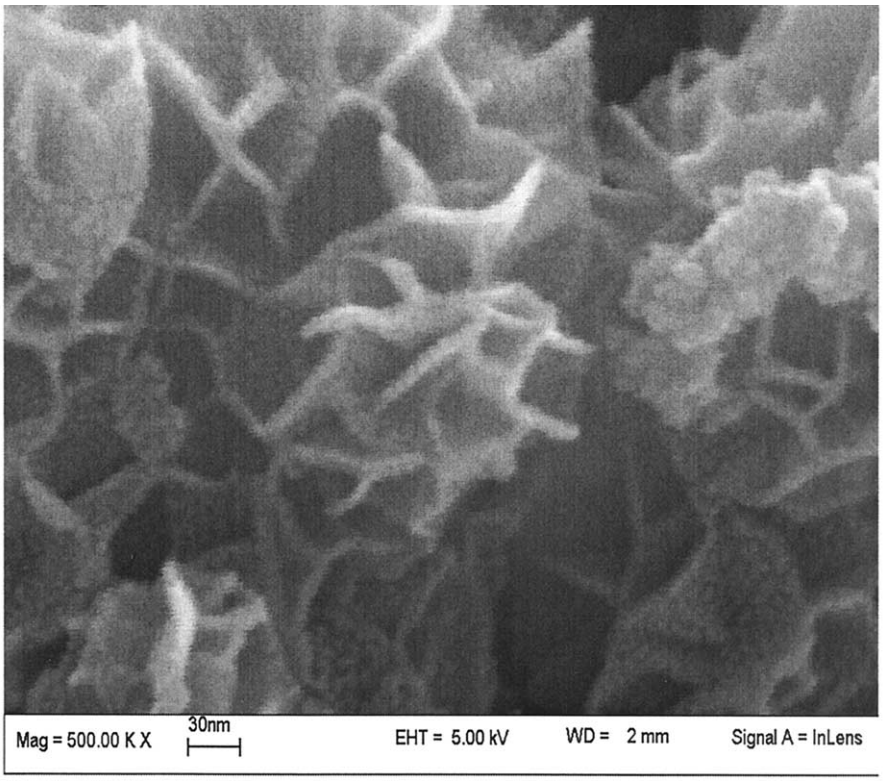

Fig. 8. High-resolution FE-SEM image of synthetic birnessite. The scale bar denotes 30 nm. The image shows that the morphology is similar to that of a barite rose. The minute bumps on the plate surfaces are due to the gold conductive coating applied to the unreacted sample before SEM imaging.

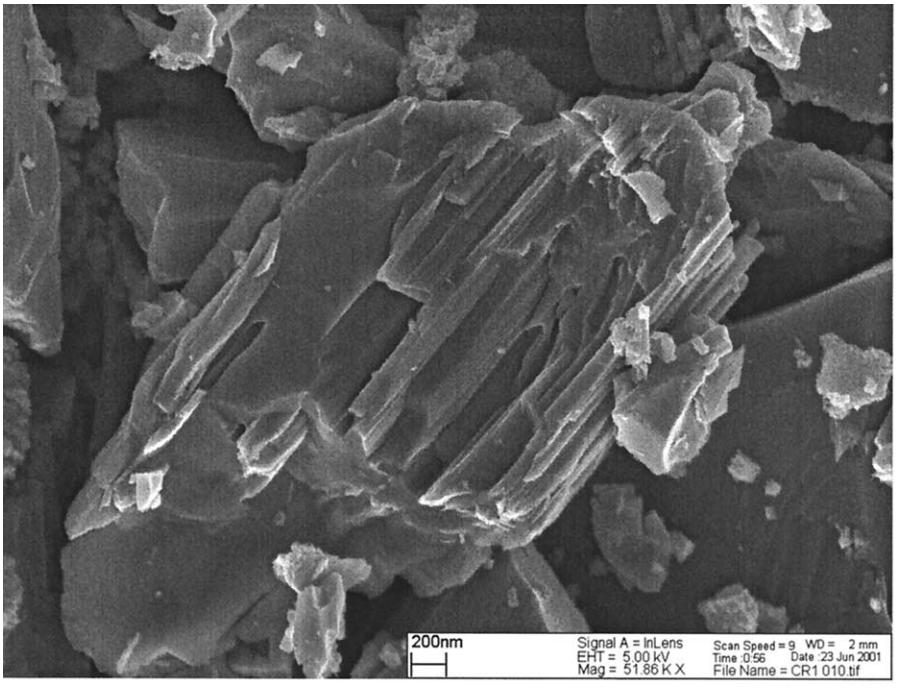

Fig. 9. FE-SEM image of natural cryptomelane, Cr1 without any conductive coating. Note the scale bar denotes 200 nm.

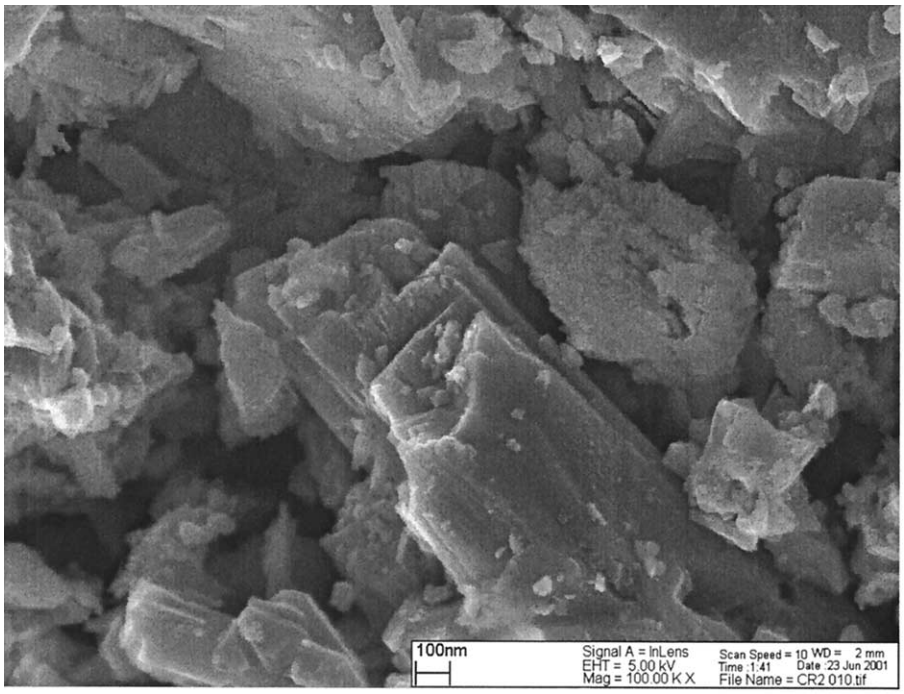

Fig. 10. FE-SEM image of natural cryptomelane, Cr2 without any conductive coating. The scale bar denotes 100 nm.

interlayers within three or four nanometers of the surface. Therefore, we can conclude that most of the Pb is in the interlayers of the birnessite structure. This clearly suggests that the high sorption efficiency of the birnessite is probably due to the additional reactive sites in the interlayer of the solid. Similarly, the synthetic cryptomelane sorbed by far the most Pb relative to the two natural ones, yet the Pb/Mn surface ratio is only slightly higher for the synthetic sample. Therefore, Pb has probably entered the synthetic cryptomelane tunnels. These conclusions are both supported by the EGME measurements which estimated a large amount of internal surface area for these solids (see below).

3.7. XRD

The reacted synthetic birnessite in both matrices and the synthetic cryptomelane in KNO_3 were X-rayed again (data not shown) after reaction to see if there were any observable phase changes. The samples were X-rayed on the filter paper with just the limited sample that was used in the reactor. A filter paper alone was also X-rayed. The filter paper caused a noticeable background hump; this hump made it more difficult to examine the birnessite pattern. However, it was clear that the 7.20 Å peak of birnessite, representing its basal spacing (Golden et al., 1986; Feng et al., 1998) was reduced to 7.06 Å for the reacted sample in the $NaNO_3$ matrix and 6.89 Å for the reacted sample in the KNO_3 matrix. This basal spacing reduction has been observed before under similar circumstances (Van der Weijden and Kruissink, 1977; McKenzie, 1980) and is an additional indication that Pb has exchanged for alkali cations in interlayer sites.

The reacted cryptomelane phase still X-rayed as cryptomelane but some of the peaks seemed slightly sharper.

3.8. Reactions in Interlayers and Tunnel Structures

Several authors have noted that birnessite readily participates in cation exchange reactions (see Post, 1992; Ching and Suib, 1997; Brock et al., 1998). However, experiments have shown that the extent of exchange is dependent upon the nature of the cation and the hydration, or lack thereof, of the interlayer (Golden et al., 1986; Ching and Suib, 1997; Brock et al., 1998). EXAFS studies revealed that Pb(II) formed inner-sphere, corner-sharing complexes located above and below vacancies in the MnO_2 layers (Morin et al., 1999; Matocha et al., 2001) and using polarized and extended XAFS Manceau et al. (2002) specifically noted octahedral tridentate corner-sharing complexes with Pb and the birnessite interlayer. Manceau et al. (2002) also noted that the EXAFS data is consistent with the formation of octahedral, tridentate edge-sharing interlayer complexes.

Members of the hollandite group such as cryptomelane are referred to by some authors as molecular sieves and it is often noted that the cryptomelane tunnel structures are capable of fixing metal ions with an effective ionic radius of approximately 1.4 Å into 4.6 Å tunnels (Feng et al., 1995a; Feng et al., 1995b; Ching and Suib, 1997; Brock et al., 1998). The ionic radii for K^+ is 1.33 Å, Pb^{2+} is 1.20 Å, Mn^{2+} is 0.80 Å, Na^+ is 0.95 Å, Mn^{4+} is 0.50 Å, and water is 1.38 Å (Bystrom and Bystrom, 1950; Murray, 1975; Van der Weijden and Kruissink, 1977). It makes sense that K is particularly suited towards cryptomelane. In hollandite and cryptomelane K occupies a

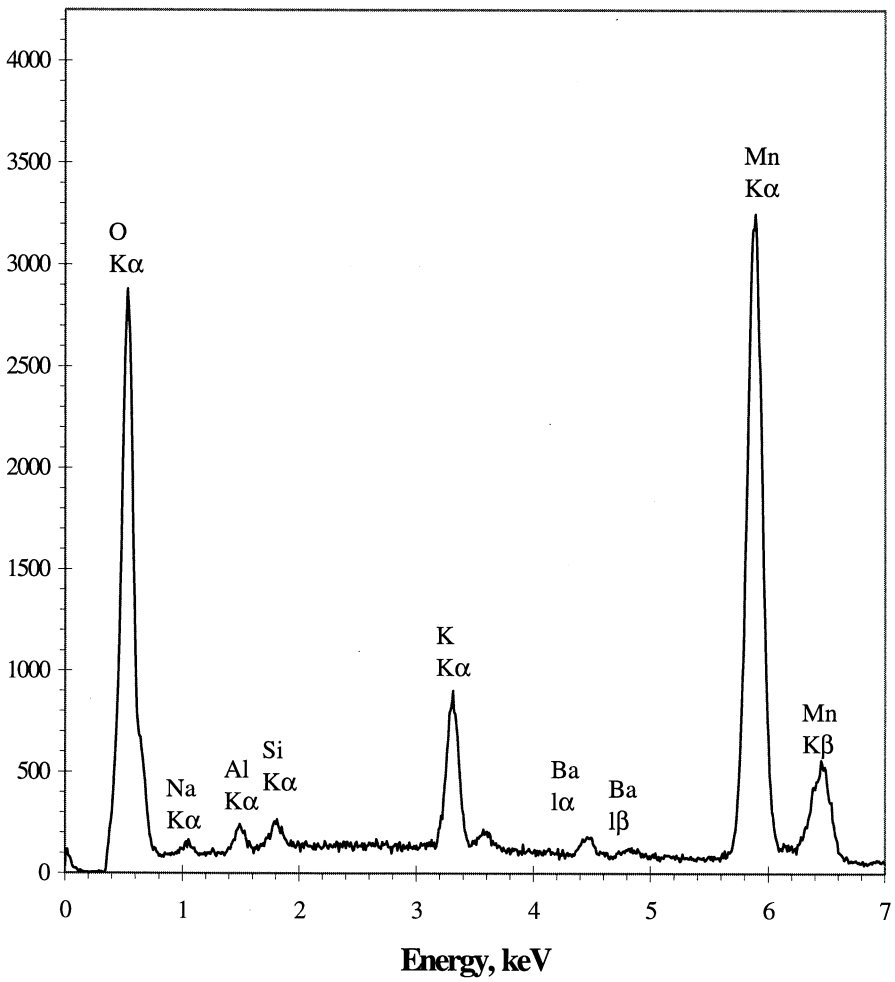

Fig. 11. EDS spectra of unreacted natural cryptomelane, Cr1.

"special position," a cavity formed by 8 O atoms at the corners of a distorted prism, whereas Pb(II) would be displaced somewhat from this position (Post et al., 1982). Bystrom and Bystrom (1950), followed by Van der Weijden and Kruissink (1977), discuss that larger ions such as K keep the cryptomelane structure from collapsing; however the K ion is somewhat too large for the structure because of the short distance between equivalent sites that accommodate the ions. Thus these authors concluded that this rationale could explain the higher exchange capacity of smaller ions, and would mean that Pb would be favored over K in an exchange reaction. Van der Weijden and Kruissink (1977) found that Pb was preferentially sorbed to birnessite, but it was not favored by poorly crystalline cryptomelane which favored larger Ba instead. Perseil and Giovanoli (1988) studied the hollandite group including intermediate members and suggested that substitution may occur in favor of the higher valence ions. McKenzie (1980) did not see a coronodite pattern for the Pb-reacted cryptomelane XRD sample, which is what one would expect if Pb significantly replaced K in the tunnels of the cryptomelane structure. Feng et al. (1995a,b) notes that the K in cryptomelane can be topotactically extracted, but it must be done in the presence of an acid. Obviously, a tunnel structure, especially a more compact tunnel structure (Giovanoli and Brutsch, 1979), is much less likely to undergo exchange than a layer structure.

To further assess the accessibility of the internal surface sites of birnessite and cryptomelane, the EGME technique was used to measure their total specific surface area. This technique is often used to measure the interlayer area of certain clay minerals. The EGME surface area of the synthetic birnessite is 375.8 m^2/g and the synthetic cryptomelane measures 261.4 m^2/g. These values are roughly an order of magnitude higher than the BET N_2 values of 35.4 and 25.7 for the synthetic birnessite and synthetic cryptomelane, respectively. If the Pb sorption data is normalized to these higher EGME values, the total Pb sorption is within range of the amount of Pb removed from solution by the Fe-oxides, emphasizing the importance of the internal surface area of the Mn-oxides for Pb sorption. However, caution must be exercised when applying EGME data to oxides as virtually no work has been done to determine the appropriateness of this method for oxides rather than clays.

4. CONCLUSIONS

The lead conclusion from this systematic study, based on natural and synthetic species of seven Mn- and Fe-oxides in

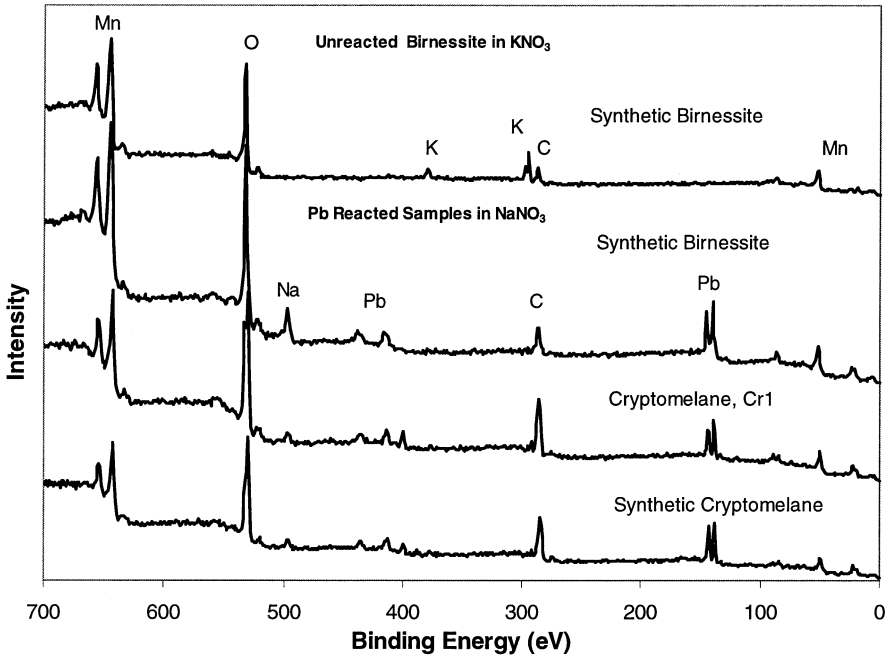

Fig. 12. XPS survey scans of unreacted synthetic birnessite (top spectrum) in KNO_3 and selected Pb reacted samples (bottom three spectrum) in $NaNO_3$ background electrolyte. Cr2 spectrum (not included here) shows the same elements in similar proportions as the Cr1 spectrum. The major peaks have been identified.

two background electrolytes, is that Mn-oxides are generally more efficient sorbents of Pb than Fe-oxides. With the exception of synthetic pyrolusite (see below), our results clearly suggest that this efficiency is directly related to internal reactive sites in the structures of Mn-oxides that contain them (birnessite and cryptomelane, in our case). Layer structures such as birnessite have the highest Pb sorption efficiency, while a 2×2 tunnel structure such as cryptomelane has lower efficiencies than birnessite, but higher efficiencies than other Mn- or Fe-oxide structures without internal reactive sites. The tunnel structures are likely more limited in efficiency than layer structures due to the steric restrictions of tunnels, which are not even cross-linked as exhibited, for example, by many zeolites.

Other important results include the observation that synthetic pyrolusite and cryptomelane have higher sorption efficiencies for Pb than their natural counterparts or natural and synthetic Fe-oxide minerals tested in this study. Overall, only the natural pyrolusite tested clearly had a sorption efficiency as low as the Fe-oxides, but one of the two natural cryptomelane samples did approach similar values. Most of the natural and synthetic Fe-oxides examined in this study removed about the same amount of Pb from solution once normalized to BET N_2 surface area, although synthetic akaganéite and hematite were significantly less reactive than the rest.

There are a number of reasons why synthetic samples might be more or less reactive than natural ones (e.g., differences in impurities, surface composition, crystal form, microtopography, and crystal size). In the case of cryptomelane, this difference may be due to tunnel exchange kinetics. The synthetic cryptomelane, which sorbed up to twice the Pb as the natural cryptomelanes in these experiments, has only K in its 2×2 tunnels at the beginning of the experiments. The natural samples have both K and Ba. Barium-oxygen bonds in the tunnels have considerably higher bond strengths relative to K-O bonds (Brese and Okeeffe, 1991), and the exchange and passage of Pb in the tunnels would therefore be expected to be slower in the presence of Ba. The fact that the synthetic pyrolusite sorbs considerably more Pb than the natural variety tested, and that its Pb sorption efficiency is so high overall, remains a mystery. Pyrolusite has a framework structure, without internal reaction sites like cryptomelane. The only unusual feature of the synthetic sample was its very low surface area, by far the lowest of all samples used in this study, but this of course was taken into account in the uptake efficiency calculation. Otherwise, its XRD pattern and composition were nominal.

Lead was shown to go into the interlayer of synthetic birnessite by comparing solution sorption data to XPS surface enrichment calculations; similar approaches suggest that Pb

Table 3. Comparison of Pb sorption data to XPS data in the $NaNO_3$ background electrolyte.

	Nat. Cryptomelane, Cr1	Nat. Cryptomelane, Cr2	Syn. Cryptomelane	Syn. Birnessite
Total Pb after 5 h (μmol/m^2)	1.46	2.72	6.95	12.38
Pb/Mn Atomic Ratio (XPS)	0.08	0.06	0.09	0.06

may be able to go into the tunnels of some cryptomelane samples, especially the synthetic sample. X-ray diffraction data did show that the interlayer spacing of the birnessite was decreasing as expected for Pb substitution. X-ray diffraction did not show a coronadite pattern replacing the cryptomelane pattern with Pb sorption; this is most likely because not enough Pb replaced the K in the interlayer to form coronadite in such a short experiment (approx. 5 h) at low temperature. Supporting this, coronadite as well as hollandite are generally formed under hydrothermal processes whereas cryptomelane is generally formed near oxidation zones (Perseil and Giovanoli, 1988). Coronadite and hollandite seem to only be formed when the Pb and Ba ions get into the tunnel structure with the aid of higher temperatures.

Overall, the sorption data does not correspond well with the IEP data suggesting that specific chemical (bonding) interactions dominate the sorption phenomena beyond the influence of electrostatic mechanisms in Pb association with the solids studied. This agrees with the current findings in the literature that Pb specifically sorbs as inner-sphere complexes to Fe and Mn-oxides. Additionally, background electrolytes cannot be considered inert in the presence of Mn-oxides as seen by the increase in the IEP data when going from $NaNO_3$ to KNO_3 electrolytes and the exchange of K for Na determined from the XPS data. The increased sorption of birnessite in the $NaNO_3$ matrix compared to the KNO_3 matrix is most likely due to Na being smaller and more labile and thus allowing Pb to exchange into the interlayer of the birnessite more easily.

This study strongly suggests that mobilized Pb in soils can be efficiently retained by Mn-oxides with internal reactive sites occupied by alkali cations, which can readily exchange out for Pb. Such strategies could be utilized in the future where Pb-contaminated sites are undergoing remediation.

Acknowledgments—This research was supported by grants from the National Science Foundation (EAR99-02996 and EAR01-03053). We would also like to thank the National Museum of Natural History of the Smithsonian Institute, the museum of the Department of Geological Sciences of Virginia Polytechnic Institute and State University, L. McKinney, D. Rimstidt, M. Eick and T. Luxton for their generous donations of mineral samples. Special thanks also go to D. Rimstidt and M. Eick for their thoughtful advice and generosity, and to L. Zelazny for the EGME measurements and valuable discussions.

Associate editor: D. Sparks

REFERENCES

Aualiitia T. U. and Pickering W. F. (1987) The specific sorption of trace amounts of Cu, Pb, and Cd by inorganic particulates. *Water Air Soil Pollut.* **35 (***1–2***)**, 171–185.

Balistrieri L. S. and Murray J. W. (1982) The surface chemistry of δ-MnO_2 in major ion seawater. *Geochim. Cosmochim. Acta* **46,** 1041–1052.

Balistrieri L. S. and Murray J. W. (1986) The surface chemistry of sediments form the Panama Basin: The influence of Mn oxides on metal adsorption. *Geochim. Cosmochim. Acta* **50,** 2235–2243.

Boeckx R. L. (1986) Lead poisoning in children. *Anal. Chem.* **58 (***2***),** 274A–287A.

Brese N. E. and O'Keeffe M. (1991) Bond-valence parameters for solids. *Acta Crystallogr. Sect. B-Struct. Commun.* **47,** 192–197.

Brock S. L., Duan N. G., Tian Z. R., Giraldo O., Zhou H., and Suib S. L. (1998) A review of porous manganese oxide materials. *Chem. Mater.* **10 (***10***),** 2619–2628.

Buck Scientific. (1992) Model 200A atomic absorption spectrophotometer flame system- instruction manual. Buck Scientific, Inc.

Buhrke V. E., Jenkins R., and Smith D. K. (1998) A practical guide for the preparation of specimens for X-ray fluorescence and X-ray diffraction analysis. John Wiley & Sons, Inc.

Burns R. G. (1976) The uptake of cobalt into ferromanganese nodules, soils, and synthetic manganese (IV) oxides. *Geochim. Cosmochim. Acta* **40,** 95–102.

Burns R. G. and Burns V. M. (1979) Manganese oxides. *Marine Minerals, Vol. 6* (ed. R. G. Burns)1–40. Mineralogical Society of America.

Bystrom A. and Bystrom A. M. (1950) The crystal structure of hollandite, the related manganese oxide minerals, and α-MnO_2. *Acta Crystallogr.* **3,** 146–154.

Carpenter R. H., Pope T. A., and Smith R. L. (1975) Fe-Mn oxide coatings in stream sediment geochemical surveys. *J. Geochem. Explor.* **4,** 349–363.

Carter D. L., Heilman M. D., and Gonzalez C. L. (1965) Ethylene glycol monoethyl ether for determining surface area of silicate minerals. *Soil Sci.* **100,** 356–360.

Chao T. T. and Theobald P. K. (1976) The significance of secondary ion and manganese oxides in geochemical exploration. *Econ. Geol.* **71,** 1560–1569.

Ching S. and Suib S. L. (1997) Synthetic routes to microporous manganese oxides. *Comment. Inorg. Chem.* **19 (***5***)**, 263–282.

Chlopecka A. and Adriano D. C. (1997) Influence of zeolite, apatite and Fe-oxide on Cd and Pb uptake by crops. *Sci. Total Environ.* **207,** 195–206.

Cornell R. M. and Schwertmann U. (1996) *The Iron Oxides: Structures, Properties, Reactions, Occurrence and Uses*. VCH Publishers.

Dahal M. P. and Lawrance G. A. (1996) Adsorption of thallium(I), lead(II), copper(II), bismuth(III) and chromium(III) by electrolytic manganese dioxide. *Adsorp. Sci. Technol.* **13 (***4***)**, 231–240.

Davies B. E. (1995) Lead. In *Heavy Metals in Soils* (ed. B. J. Alloway) pp. 206–223. Chapman & Hall.

Dixon J. B. and Skinner H. C. W. (1992) Manganese minerals in surface environments. In *Biomineralization Processes of Iron and Manganese: Modern and Ancient Environments*, Vol. 21 (ed. H. C. W. Skinner and R. W. Fitzpatrick), pp. 51–73. Catena Verlag.

Dong D. M., Nelson Y. M., Lion L. W., Shuler M. L., and Ghiorse W. C. (2000) Adsorption of Pb and. Cd onto metal oxides and organic material in natural surface coatings as determined by selective extractions: new evidence for the importance of Mn and Fe oxides. *Water Res.* **34 (***2***)**, 427–436.

Dong D., Li Y., Zhang B., Hua X., and Yue B. (2001) Selective chemical extraction and separation of Mn, Fe oxides and organic material in natural surface coatings: Application to the study of trace metal adsorption mechanism in aquatic environments. *Microchem. J.* **69,** 89–94.

Feng Q., Kanoh H., Miyai Y., and Ooi K. (1995a) Alkali-metal ions insertion/extraction reactions with Hollandite-type manganese oxide in the aqueous-phase. *Chem. Mater.* **7 (***1***),** 148–153.

Feng Q., Kanoh H., Miyai Y., and Ooi K. (1995b) Hydrothermal synthesis of lithium and sodium manganese oxides and their metal-ion extraction insertion reactions. *Chem. Mater.* **7 (***6***),** 1226–1232.

Feng Q., Yanagisawa K., and Yamasaki N. (1998) Hydrothermal soft chemical process for synthesis of manganese oxides with tunnel structures. *J. Porous Mater.* **5 (***2***),** 153–161.

Garrels R. M. and Christ C. L. (1965) *Solutions, Minerals and Equilibria*. Freeman, Cooper & Company.

Gadde R. R. and Laitinen H. A. (1974) Studies of heavy metal adsorption by hydrous iron and manganese oxides. *Anal. Chem.* **46 (***13***),** 2022–2026.

Gilmore E. A., Evans G. J., and Ho M. D. (2001) Radiochemical assessment of the readsorption and redistribution of lead in the SM&T sequential extraction procedure. *Anal. Chim. Acta* **439,** 139–151.

Giovanoli R. and Brutsch R. (1979) L'echange des ions de transition par le manganate- 10 Å et le manganate 7 Å. In *La Genese Des Nodules De Manganese*, Vol. 289 (ed. C. I. d. C.N.R.S.), pp. 305–315. Colloques Internatonaux du C.N.R.S.

Golden D. C., Dixon J. B., and Chen C. C. (1986) Ion exchange thermal transformations and oxidizing properties of birnessite. *Clays Clay Miner.* **34 (***5***),** 511–520.

Goldstein J. I., Romig A. D., Jr., Newbury D. E., Lyman C. E., Echlin P., Fiori C., Joy D. C., and Lifshin E. (1992) *Scanning electron microscopy and x-ray microanalysis: A text for biologists, materials scientists, and geologists*. Plenum Press.

Gregson S. K. and Alloway B. J. (1984) Gel-permeation chromatography studies on the speciation of lead in solutions of heavily polluted soils. *J. Soil Sci.* **35**(1), 55–61.

Healy T. W., Herring A. P., and Fuerstenau D. W. (1966) The effect of crystal structure on the surface properties of a series of manganese dioxides. *J. Colloid Interface Sci.* **21,** 435–444.

Hudson-Edwards K. A. (2000) Heavy metal-bearing Mn oxides in river channel and floodplain sediments. In *Environmental Mineralogy: Microbial Interactions, Anthropogenic Influences, Contaminated Land and Waste Management*, Vol. 9 (ed. J. D. Cotter-Howells, L.S. Campbell, E. Valsami-Jones, and M. Batchelder), pp. 207–226. Mineralogical Society of Great Britian & Ireland.

Jenne E. A. (1968) Controls on Mn, Fe, Co, Ni, Cu, and Zn concentrations in soils and water: The significant role of hydrous Mn and Fe oxides. In *Trace Inorganics in Water*, Vol. 73 (ed. R. A. Baker) pp. 337–387. American Chemical Society.

Junta J. and Hochella M. F. (1994) Manganese(II) oxidation at mineral surfaces- a microscopic and spectroscopic study. *Geochim. Cosmochim. Acta* **58,** 4985–4999.

Kabata-Pendias A. (1980) Heavy metals sorption by clay minerals and oxides or iron and manganese. *Mineralogia Polonica* **11 (***2***)**, 3–13.

Kaim W. (1994) *Bioinorganic Chemistry: Inorganic Elements in the Chemistry of Life: An Introduction and Guide*. John Wiley & Sons.

Kosmulski M. (2001) *Chemical Properties of Material Surfaces*. Marcel Dekker, Inc.

Langmuir D. (1997) *Aqueous Environmental Geochemistry*. Prentice-Hall, Inc.

Li Y. H. (1982) Interelement relationship in abyssal Pacific ferromanganese nodules and associated pelagic sediments. *Geochim. Cosmochim. Acta* **46,** 1053–1060.

Manceau A., Charlet L., Boisset M. C., Didier B., and Spadini L. (1992) Sorption and speciation of heavy metals on hydrous Fe and Mn oxides. From microscopic to macroscopic. *Appl. Clay Sci.* **7,** 201–223.

Manceau A., Drits V. A., Silvester E., Bartoli C., and Lanson B. (1997) Structural mechanism of Co^{2+} oxidation by the phyllomanganate buserite. *Am. Mineral.* **82 (***11–12***)**, 1150–1175.

Manceau A., Lanson B., and Drits V. A. (2002) Structure of heavy metal sorbed birnessite. Part III: Results from powder and polarized extended X-ray absorption fine structure spectroscopy. *Geochim. Cosmochim. Acta* **66 (***15***)**, 2639–2663.

Matocha C. J., Elzinga E. J., and Sparks D. L. (2001) Reactivity of Pb(II) at the Mn(III,IV) (Hydr)oxide-water interface. *Environ. Sci. Technol.* **35,** 2967–2972.

McBride M. B. (1994) *Environmental Chemistry of Soils*. Oxford University Press.

McCarty D. K., Moore J. N., and Marcus W. A. (1998) Mineralogy and trace element association in an acid mine drainage iron oxide precipitate; comparison of selective extractions. *Appl. Geochem.* **13 (***2***)**, 165–176.

McKenzie R. M. (1971) The synthesis of birnessite, cryptomelane, and some other oxides and hydroxides of manganese. *Mineral. Mag.* **38 (***296***)**, 493–502.

McKenzie R. M. (1978) The effect of two manganese dioxides on the uptake of lead, cobalt, nickel, copper and zinc by subterranean c lover. *Aust. J. Soil Res.* **16 (***2***)**, 209–214.

McKenzie R. M. (1980) The adsorption of lead and other heavy metals on oxides of manganese and iron. *Aust. J. Soil Res.* **18 (***1***)**, 61–73.

McKenzie R. M. (1981) The surface charge on manganese dioxides. *Aust. J. Soil Res.* **19**, 41–50.

McKenzie R. M. (1989) Manganese oxides and hydroxides. In *Minerals in Soil Environments*, Vol. 1 (ed. J. B. Dixon and S. B. Weed) pp. 437–465. Soil Science Society of America.

Morin G., Ostergren J. D., Juillot F., Ildefonse P., Calas G., and Brown G. E. (1999) XAFS determination of the chemical form of lead in smelter- contaminated soils and mine tailings: Importance of adsorption processes. *Am. Mineral.* **84 (***3***)**, 420–434.

Murray J. W. (1974) The surface chemistry of hydrous manganese dioxide. *J. Colloid Interface Sci.* **46 (***3***)**, 357–371.

Murray J. W. (1975) The interaction of metal ions at the manganese dioxide-solution interface. *Geochim. Cosmochim. Acta* **30**, 505–519.

Norrish K. (1975) Geochemistry and mineralogy of trace elements. In *Trace Elements in Soil-Plant-Animal Systems* (ed. D. J. D. Nicholas and A. R. Egan) pp. 55–81. Academic Press.

Nriagu J. O. (1978) Lead in soils, sediments and major rock types. In *The Biogeochemistry of Lead in the Environment: Ecological Cycles*, Vol. 1 A (ed. J. O. Nriagu) pp. 16–72. Elsevier/North-Holland Biomedical Press.

O'Reilly S.E. (2002) Lead sorption efficiencies of natural and synthetic Mn and Fe-oxides. Electronic dissertation, Virginia Polytechnic Institute and State University.

Ostergren J. D., Brown G. E., Parks G. A., and Tingle T. N. (1999) Quantitative speciation of lead in selected mine tailings from Leadville, CO. *Environ. Sci. Technol.* **33 (***10***)**, 1627–1636.

Parida K., Satapathy P. K., and Das N. (1996) Studies on Indian Ocean manganese nodules. Adsorption of some bivalent heavy metal ions onto ferromanganese nodules. *J. Colloid Interface Sci.* **181 (***2***)**, 456–462.

Paulson A. J., Feely R. A., Curl H. C., Crecelius E. A., and Geiselman T. (1988) The impact of scavenging on trace-metal budgets in Puget Sound. *Geochim. Cosmochim. Acta* **52 (***7***)**, 1765–1779.

Perseil E. and Giovanoli R. (1988) Sur la variation de la composition ponctuelle des termes de las serie isostructurale: Cryptomelane-Hollandite-Cornodite et les conditions de gisement. *Schweiz. Mineral. Petrogr. Mitt.* **68**, 113–123.

Post J. E. (1992) Crystal structures of manganese oxide minerals. In *Biomineralization Processes of Iron and Manganese: Modern and Ancient Environments*, Vol. 21 (ed. H. C. W. Skinner and R. W. Fitzpatrick) pp. 51–73. Catena Verlag.

Post J. E., Von Dreele R. B., and Buseck P. R. (1982) Symmetry and cation displacements in hollandites: Structure refinements of hollandite, cryptomelane and priderite. *Acta Crystallogr.* **B38**, 1056–1065.

Rauch S., Morrison G. M., Motelica-Heino M., Donard O. F. X., and Muris M. (2000) Elemental association and fingerprinting of traffic related metals in road sediments. *Environ. Sci. Technol.* **34 (***15***)**, 3119–3123.

Rickard D. T. and Nriagu J. O. (1978) Aqueous environmental chemistry of lead. In *The Biogeochemistry of Lead in the Environment: Ecological Cycles*, Vol. 1 A (ed. J. O. Nriagu) pp. 219–284. Elsevier/North-Holland Biomedical Press.

Rimstidt J. D. and Newcomb W. D. (1993) Measurement and analysis of rate data: The rate of reaction of ferric ion with pyrite. *Geochim. Cosmochim. Acta* **57**, 1919–1934.

Schwertmann U. and Cornell R. M. (1991) *Iron Oxides in the Laboratory*. VCH Publishers.

Schwertmann U. and Taylor R. M. (1989) Iron oxides. In *Minerals in Soil Environments*, Vol. 1 (ed. J. B. Dixon and S. B. Weed) pp. 379–438. Soil Science Society of America.

Sparks D. L. (1995) *Environmental Soil Chemistry*. Academic Press.

Tampouris S., Papassiopi N., and Paspaliaris I. (2001) Removal of contaminated metals from fine grained soils, using agglomeration, chloride solutions and pile leaching techniques. *J. Haz. Mater.* **B84**, 297–319.

Taylor R. M. and McKenzie R. M. (1966) The association of trace elements with manganese minerals in Australian soils. *Aust. J. Soil Res.* **4**, 29–39.

Taylor R. M., McKenzie R. M., and Norrish K. (1964) The mineralogy and chemistry of manganese in some Australian soils. *Aust. J. Soil Res.* **2**, 235–248.

Van der Weijden C. H. and Kruissink E. C. (1977) Some geochemical controls on lead and barium concentrations in ferromanganese deposits. *Mar. Chem.* **5**, 93–112.

Waltham C. A. and Eick M. J. (2002) Kinetics of arsenic adsorption on goethite in the presences of sorbed silicic acid. *Soil Sci. Soc. Am. J.* **66**, 818–825.

Weaver R. (2001) Comparison of the reactivity of various Mn-oxides with Cr(III) aqueous: Microscopic and spectroscopic observations of dissolution, Cr-sorption and Cr & Mn redox interactions. Electronic dissertation, Virginia Polytechnic Institute and State University.

webmineral.com. (2002) Akaganéite Mineral Data, http://webmineral.com/data/Akaganeite.shtml.

Welz B. and Sperling M. (1999) *Atomic Absorption Spectrometry*. Wiley-VCH.

Yang D. S. and Wang M. K. (2002) Synthesis and characterization of birnessite by oxidizing pyrochroite in alkaline conditions. *Clays Clay Miner.* **50 (*1*)**, 63–69.

Yousef A. A., Arafa M. A., and Malati M. A. (1971) Adsorption of sulfite, oleate and manganese (II) ions by β-manganese dioxide and its activation in flotation. *Journal of Appl. Chem. Biotech.* **21**, 200–207.

Zelazny L., He L., and Vanwormhoudt A. (1996) Charge analysis of soils and anion exchange. In *Methods of Soil Analysis: Chemical Methods Part 3*, Vol. 5 (ed. D. L. Sparks) pp. 1231–1253. Soil Science Society of America.